# Short-term forecasting of PM$_{10}$ and PM$_{2.5}$ concentrations with Facebook's Prophet Model at the Belgrade-Zeleno brdo

*Filip Arnaut* [1] 🆔 *, Vesna Cvetkov* [1] 🆔 *, Dragana Đurić* [1] 🆔
*and Mileva Samardžić-Petrović* [2] 🆔

[1] Department of Geophysics, Faculty of Mining and Geology, University of Belgrade, Belgrade, Serbia

[2] Department of Geodesy and Geoinformatics, Faculty of Civil Engineering, University of Belgrade, Belgrade, Serbia

We demonstrate the use of Facebook's Prophet (usually just called Prophet) model for short-term air quality forecasting at Belgrade-Zeleno brdo monitoring station. To address missing data, we applied minimally-altering data distribution imputation techniques. Linear interpolation proved effective for short-term gaps (1–3 hours), hourly mean method for mid-term gaps (24–26 hours), and Hermite interpolation polynomial for long-term gaps (132–148 hours). The most significant data change was a 3.4% shift in skewness. Partitioning the time series enabled a detailed quality assessment of the Prophet model, with PM$_{2.5}$ predictions being more precise than PM$_{10}$. Using the longest time series for forecasting yielded absolute errors of 6.5 μg/m$^3$ for PM$_{10}$ and 2.7 μg/m$^3$ for PM$_{2.5}$. Based on 173 forecasts, we anticipate Prophet model root-mean-square values under 6.26 μg/m$^3$ and 9.99 μg/m$^3$ for PM$_{2.5}$ and PM$_{10}$ in 50% of cases. The Prophet model demonstrates several advantages and yields satisfactory results. In future research, the results obtained from the Prophet model will serve as benchmark values for other models. Additionally, the Prophet model is capable of providing satisfactory air quality forecasting results and will be utilized in future research.

*Keywords*: time series analysis, time series forecasting, air quality, suspended particles

## 1. Introduction

The Republic of Serbia (RS) has seen an increase in the demand for electric energy, in alignment with the global trend. This trend is particularly pronounced in the densely populated and urbanized region of the capital city of Belgrade. In the RS, lignite thermal power plants are the primary source of electricity (Energy Agency of the Republic of Serbia, 2020), resulting in the production of large quantities of suspended particles, especially PM$_{10}$ and PM$_{2.5}$. Most of the electricity produced in the RS is derived from fossil fuels such as coal and natural gas, with renewable sources accounting for 20% of the total (Official Gazette of the Republic of Serbia, 156/2020). Notably, five of the

ten most polluting thermal power plants are in the RS, while the average Western Balkan thermal power plant emits 16 times more suspended particles than the average European Union thermal power plant (Puljić et al., 2019).

The ecological problem posed by suspended particles in the RS, resulting from an insufficiently regulated energy sector, is further exacerbated in urban environments by traffic and heating materials. A substantial body of research has established a strong link between increased suspended particle concentrations and cardiovascular diseases, as well as an increased susceptibility to allergens (Jovanović, 2020; Dockery et al., 1992; Araujo, 2011; Bernstein et al., 2011). According to calculations by the World Health Organization for the year 2019, based on data from 2012, approximately 5400 fatalities and 126,000 lost years of life can be attributed to the rise in airborne particles (World Health Organization, 2019).

The knowledge of the spatial distribution of suspended particles in the future can be a crucial piece of information for decision -makers. Since 1927 (Bisgaard and Kulachi, 2011), modern methods of time series forecasting have been developed, and today there are, numerous models and methods for the forecasting of time series data, ranging from the simplest to the most complex, such as machine learning approaches.

The Prophet model was selected for this study due to its numerous successful applications in forecasting air pollution parameters in large urban areas worldwide. Additionally, other studies have shown that the Prophet model exhibits notable capabilities in predicting various time-series data, such as district heating load (Shakeel et al., 2023a, b) and the percentage of COVID-19 infected population (Papastefanopoulos et al., 2020). Notably, the Prophet model has exhibited superior performance compared to traditional machine learning models, particularly in scenarios with limited data availability. For instance, research conducted in Seoul (South Korea) demonstrated short-term and long-term forecasts of PM$_{10}$, PM$_{2.5}$, O$_3$, NO$_2$, SO$_2$, and CO concentrations using the Prophet model (Shen et al. 2020). The mean absolute error values obtained for PM$_{2.5}$ and PM$_{10}$ concentrations were 12.6 μg/m$^3$, and 19.6 μg/m$^3$, respectively. The data were two to four times more accurate than similar models' forecasts (Shen et al., 2020). In Zhao et al. (2018), the Prophet model was instrumental in revealing data trends that might otherwise be challenging to discern. The study found that the highest annual PM$_{2.5}$ levels occur in January, with the highest weekly levels on Fridays, and the lowest concentrations on Sundays and Mondays (Zhao et al., 2018). Hybrid forecasting methods were also shown to yield more accurate results compared to simple methods when forecasting PM$_{2.5}$ concentrations (Ejohwomu et al., 2022). The forecasts were quantified using the mean absolute scaled error (Hyndman and Koehler, 2006), a reliable method for assessing forecast model quality when comparing multiple models. Samal et al. (2019) demonstrated that the Prophet model without transformations provided more accurate air

quality forecasts in Bhubaneswar, India, compared to the Seasonal ARIMA (SARIMA) model. The addition of log transformation further improved the Prophet model's accuracy (Samal et al., 2019). Ye (2019) introduced a hybrid, weight-based model for air quality forecasting in Shenzen, China, combining the ARIMA and Prophet models for a three-day forecasting horizon. The limitations of the ARIMA model include the time-consuming search for optimal (p, d, q) parameters. The forecasting method, in general, faces challenges when predicting over long horizons, with the potential for significant model errors (Ye, 2019). The automation of the lengthy search for optimal ARIMA parameters can be achieved through the utilization of the pmdarima library in Python (Smith and Taylor, 2017). In Nanjing, China, Zhou et al. (2020) developed a hybrid Prophet-LSTM (Long Short-Term Memory) model that improved the Prophet model's accuracy, particularly for high-value predictions with a one-year forecasting horizon. Tejasvini et al. (2020) found that when comparing the Prophet model to ARIMA and Naïve Bayes, the Prophet model required the least time for making predictions and had the lowest calculated error parameter when forecasting atmospheric CO.

The primary objective of this study is to apply the Prophet model to concentration data of $PM_{10}$ and $PM_{2.5}$ suspended particles at the Belgrade-Zeleno brdo monitoring station. In this study, a more conservative approach was taken to forecasting, *i.e.*, the forecasting horizon wasn't set too far in the future but was limited to 24 hours. This approach allows us to assess the Prophet model's performance in providing satisfactory one-day-ahead forecasts—a best-case scenario. As demonstrated by Shen et al. (2020), extending the forecasting horizon can compound error terms, making a shorter horizon a more reliable measure of the model's effectiveness.

## 2. Methodology and data

Time series forecasting encompasses a range of techniques for predicting future observations based on past (historical) data. Typically, time series forecasting techniques rely on equally spaced data (Kovačić, 1995; Lütkepohl and Kratzig, 2004; Agrawal and Adhikary, 2013). While the Prophet model does not necessitate equally spaced data, this research addresses missing observations to facilitate future correlation with other models that do require equally spaced data.

The data preprocessing scheme requires information on three key parameters:

- the number of data points; the quantity of data points contained in the data file,

- the total number of data points for the investigated period; the total number of data points for the investigated period minus the number of

data points that include missing observations, or the number of data points that can be found in the time interval if no observations are missed,

- the total number of missing observations; the number of observations that were either not measured (due to instrument failure) or were eliminated from the data set (erroneous values which can also be due to instrumental failure).

The choice between data imputation, data amputation, or a combination of these methods depends on the number of missing observations and their location in the data set.

Methods for imputation of missing data can be straightforward, such as last observation carried forward, previous measurement carried backward, average method (Kang, 2013), K nearest neighbors, linear (or any other) interpolation, etc. It is essential to note that there is no "one-size-fits-all" approach to data preprocessing that is appropriate in every circumstance. Usually, imputation methods are selected by trial and error. Suitable imputation methods for this study were those that do not alter the basic statistical properties of the data *i.e.*, the data distribution after preprocessing (Fig. 1). Additionally, data amputation methods involve eliminating observations from the data set.

Both before and after data preprocessing, descriptive statistics were used to calculate various statistics, including the mean, median, mode, minimum, maximum, skewness, kurtosis, and Pearson's and Spearman's correlation coefficients between variables (Schober et al., 2018). Furthermore, a visual inspection is always valuable for checking data and its distribution (Bisgaard, Kulachi, 2011). As part of the descriptive statistics step, a quantitative approach to testing data distribution modality, based on Hartigan and Hartigan's unimodality test (Hartigan, Hartigan, 1985), was also implemented (refer to Fig. 1).

For the quantitative evaluation of the chosen model, the in-sample forecasting technique was utilized for statistical validation. In-sample forecasting was performed by removing a specific amount of data (in this case, the last 24 hours), and statistical validation was based on the discrepancy between the forecast and the removed in-sample data.

The quantitative assessment parameters for the model were the absolute error (*AE*), mean absolute error (*MAE*), absolute percentage error (*APE*), mean absolute percentage error (*MAPE*), and root mean square error (*RMSE*) are.

Absolute error (*AE*) and absolute percentage error (*APE*) are given as:

$$AE = \left| y_{forecast} - y_{true} \right| \ [\mu g/m^3] \ , \tag{1}$$
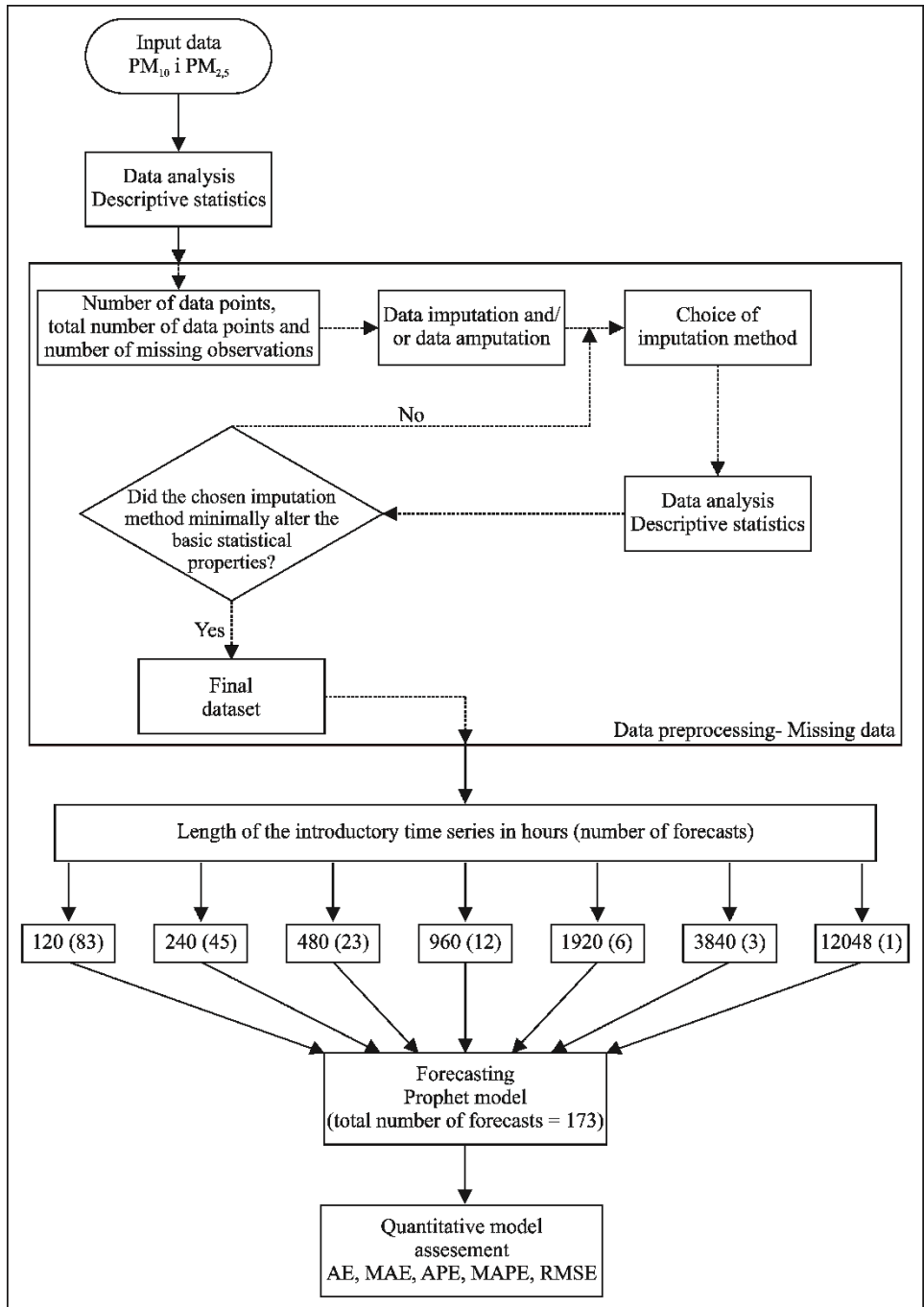
**Figure 1.** Research methodology.

$$APE = \frac{|y_{forecast} - y_{true}|}{y_{true}} \cdot 100 \ [\%], \tag{2}$$

where $y_{forecast}$ is the value predicted by the Prophet model and $y_{true}$ is the true value used for validation.

If the length of the forecasting horizon is greater than one, two additional parameters can be obtained: the mean absolute error (*MAE*) and the mean absolute percentage error (*MAPE*), which are given as:

$$MAE = \frac{\sum_{i=1}^{N} |y_{forecast} - y_{true}|}{N} \ [\mu g/m^3], \tag{3}$$

$$MAPE = \frac{\sum_{i=1}^{N} \frac{|y_{forecast} - y_{true}|}{y_{true}}}{N} \cdot 100 \ [\%], \tag{4}$$

where $N$ is the length of the forecasting horizon.

The root mean square error (*RMSE*) is defined by:

$$RMSE = \sqrt{\frac{\sum_{i=1}^{N} (y_{true} - y_{forecast})^2}{N}} \ [\mu g/m^3]. \tag{5}$$

The regression-based Prophet model (Taylor, Letham, 2018) used in this study is represented by the following equation:

$$y(t) = g(t) + s(t) + h(t) + \epsilon_t, \tag{6}$$

where $g(t)$ is the trend, $s(t)$ is the periodic, *i.e.*, seasonal variations, $h(t)$ is the non-equally spaced holiday effect, and $\epsilon_t$ are changes to which the model does not adapt to (Taylor, Letham, 2018). The Prophet model's advantages can be seen in its simplicity and its speed in processing large amounts of data.

Furthermore, it is important to note that the Prophet model does not fall under the category of machine learning models. Instead, it is more closely related to classical time series forecasting methods. Moreover, the Prophet model does not necessitate the use of a machine learning format that involves features and targets, as is typically seen in supervised machine learning algorithms. The Prophet model requires a minimum of two values as input: the *ds* value, which represents the date value for each data point, and the *y* value, which represents the measured or observed parameter that is the main focus of the forecasting process.

The PM$_{10}$ and PM$_{2.5}$ concentrations for the monitoring station Belgrade-Zeleno brdo are obtained from the Environmental Protection Agency of the Republic of Serbia for the period from January 1st, 2021, to August 17th, 2022. Measurements at the monitoring station Zeleno brdo are conducted at an hourly interval. The monitoring station is located at an elevation of 240 m in a suburban area and is part of the SEPA network (Environmental Protection Agency, 2020). Furthermore, the Zeleno brdo measuring station was selected

due to its location in a relatively undisturbed and suburban area, which is advantageous for benchmark research. The measured values of $PM_{10}$ and $PM_{2.5}$ were inspected by the Environmental Protection Agency for possible erroneous values.

The Iowa Environmental Mesonet (2022) provided hourly temperature measurements from Nikola Tesla International Airport in Belgrade, Serbia. While data from a location closer to the particle monitoring station was unavailable, data from Belgrade Airport was deemed sufficient. Notably, the distance by air between the international airport in Belgrade and the monitoring station is 18.7 km, which is acceptable under the circumstances

## 3. Results and discussion

### 3.1. Data preprocessing and exploratory data analysis

The graphical representation (Fig. 2) illustrates four distinct categories of missing observations during the data period. The number of short-term missing observations was six, with the first category encompassing missing data for 1 to 3 hours. Mid-term missing observations spanned 24 to 26 hours. The final two categories represented long-term (132 to 148 hours) and extremely long-term missing observations (2,171 hours). In total, there were 2,509 missing observations, equivalent to 17.6% of the total data.
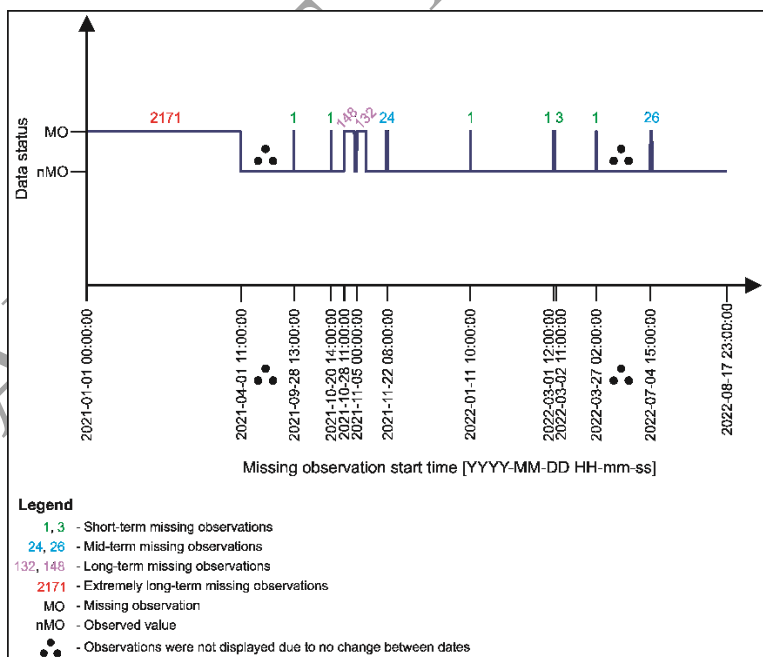


**Figure 2.** The distribution of missing observations.

The initial step in data preprocessing consisted of a conditional data amputation, *i.e.*, the reduction of the data set so that the first data would be collected on April 2, 2021. The number of missing observations has been reduced to 338 hours, or 2.8% of the reduced time interval. In the first stage, short-term missing observations were imputed, and in the final stage, long-term missing observations were imputed. The amputated data set formed the basis for the statistical parameters used in data imputation (Tab. 1).

Table 1. Statistical parameters during data imputation; T- the distribution is unimodal; CC-correlation coefficient.

| Method | Input data | | Linear interpolation | | Hourly average | | Hermite polynomial | |
|---|---|---|---|---|---|---|---|---|
| Length of missing observations | / | | Short-term | | Mid-term | | Long-term | |
| Parameter | PM$_{10}$ | PM$_{2.5}$ | PM$_{10}$ | PM$_{2.5}$ | PM$_{10}$ | PM$_{2.5}$ | PM$_{10}$ | PM$_{2.5}$ |
| Number of data points [/] | 11746 | 11746 | 11754 | 11754 | 11804 | 11804 | 12084 | 12084 |
| Minimum [µg/m$^3$] | 2.97 | 1.94 | 2.97 | 1.94 | 2.97 | 1.94 | 2.97 | 1.94 |
| Maximum [µg/m$^3$] | 218.00 | 156.00 | 218.00 | 156.00 | 218.00 | 156.00 | 218.00 | 156.00 |
| Mean [µg/m$^3$] | 26.44 | 18.69 | 26.44 | 18.69 | 26.44 | 18.69 | 26.53 | 18.85 |
| Median [µg/m$^3$] | 22.40 | 14.60 | 22.40 | 14.60 | 22.50 | 14.60 | 22.50 | 14.70 |
| Mod [µg/m$^3$] | 21.50 | 11.00 | 21.50 | 11.00 | 21.50 | 11.00 | 21.50 | 11.00 |
| Skewness [/] | 2.39 | 2.07 | 2.39 | 2.07 | 2.40 | 2.08 | 2.37 | 2.07 |
| Kurtosis [/] | 11.20 | 6.30 | 11.20 | 6.30 | 11.26 | 6.34 | 10.82 | 6.13 |
| Unimodality test [/] | T | | T | | T | | T | |
| Pearson's CC [/] | 0.87 | | 0.87 | | 0.87 | | 0.87 | |
| Spearman's CC [/] | 0.87 | | 0.87 | | 0.87 | | 0.87 | |

For short-term missed observations, the last observation carried forward method was primarily used. This method was less efficient than the linear interpolation method because linear interpolation did not alter the basic statistical parameters, it was the optimal method for short-term imputation.

The method employed for addressing mid-term missing observations involved mean substitution with the condition that hourly means were calculated. The hourly mean substitution method permits hourly variations in the PM$_{10}$ and PM$_{2.5}$ parameters throughout the day, whereas the conventional mean substitution method does not. In the median value of the PM$_{10}$ parameter, as well as the skewness and kurtosis parameters for both the PM$_{10}$ and PM$_{2.5}$ parameters, the discrepancy between the basic descriptive statistics computed prior to data imputation for the mid-term missing observations was evident. However, these discrepancies did not exceed 0.7%.

The application of K nearest neighbors and the mean substitution method for long-term data imputation first exhibited its inadequacies in the modification of the $PM_{10}$ and $PM_{2.5}$ parameter distributions. Visual analysis and Hartigan and Hartigan's unimodality test (Hartigan, Hartigan, 1985) indicated that the fundamental descriptive statistical parameters exhibited a unimodal distribution with a tail extending toward positive values (positively skewed). However, after imputation using the mean substitution method and K nearest neighbors for long-term missing observations, the distribution became bimodal. Consequently, these two methods were automatically dismissed. Several interpolation methods were assessed, and Hermite's interpolation polynomial was chosen based on its minimal deviation from the fundamental statistical properties. The kurtosis parameter, with a change of 3.39%, exhibited the most significant alteration. For a visual representation of the preprocessed data for the $PM_{10}$ and $PM_{2.5}$ parameters, refer to Fig. 3.

Additionally, at the Zeleno brdo monitoring station, the Pearson's and Spearman's correlation coefficients show 0.87 correlation between $PM_{10}$ and $PM_{2.5}$ particles. This correlation falls within the range defined as a strong positive correlation according to Schober et al. (2018).

The processed $PM_{10}$ and $PM_{2.5}$ data (Figs. 3b and 3d) exhibit an intriguing trend from October 2021 to May 2021. The increased values of suspended particles measured at the Belgrade-Zeleno brdo monitoring station may be attributable to the increased use of home heating materials during the winter months. Correlation analysis, using Pearson's and Spearman's correlation coefficients, revealed that $PM_{10}$ particles have a –0.25 (Pearson) and –0.26 (Spearman) correlation with temperature, while the correlation between $PM_{2.5}$ particles and temperature is –0.52 (Pearson) and –0.56 (Spearman). According to the correlation ranges provided by Schober et al. (2018), $PM_{10}$ particles have a weakly negative correlation with temperature, whereas $PM_{2.5}$ particles have a moderately negative correlation. The calculated correlation can be interpreted because the Pearson and Spearman correlation coefficients for both variables are comparable, *i.e.*, are within a close range. At the Belgrade-Zeleno brdo monitoring station, the onset of winter is accompanied by a moderate increase in $PM_{2.5}$ particles and a slight increase in the heavier $PM_{10}$ particles, which can be attributed to the increased use of home heating materials. In this context, it's worth noting that home heating materials have a greater effect on $PM_{2.5}$ particles than $PM_{10}$ particles.

Based on the processed $PM_{10}$ and $PM_{2.5}$ data and the air pollution index from the Environmental Protection Agency (2022), the duration of each index was displayed in Tab. 2.
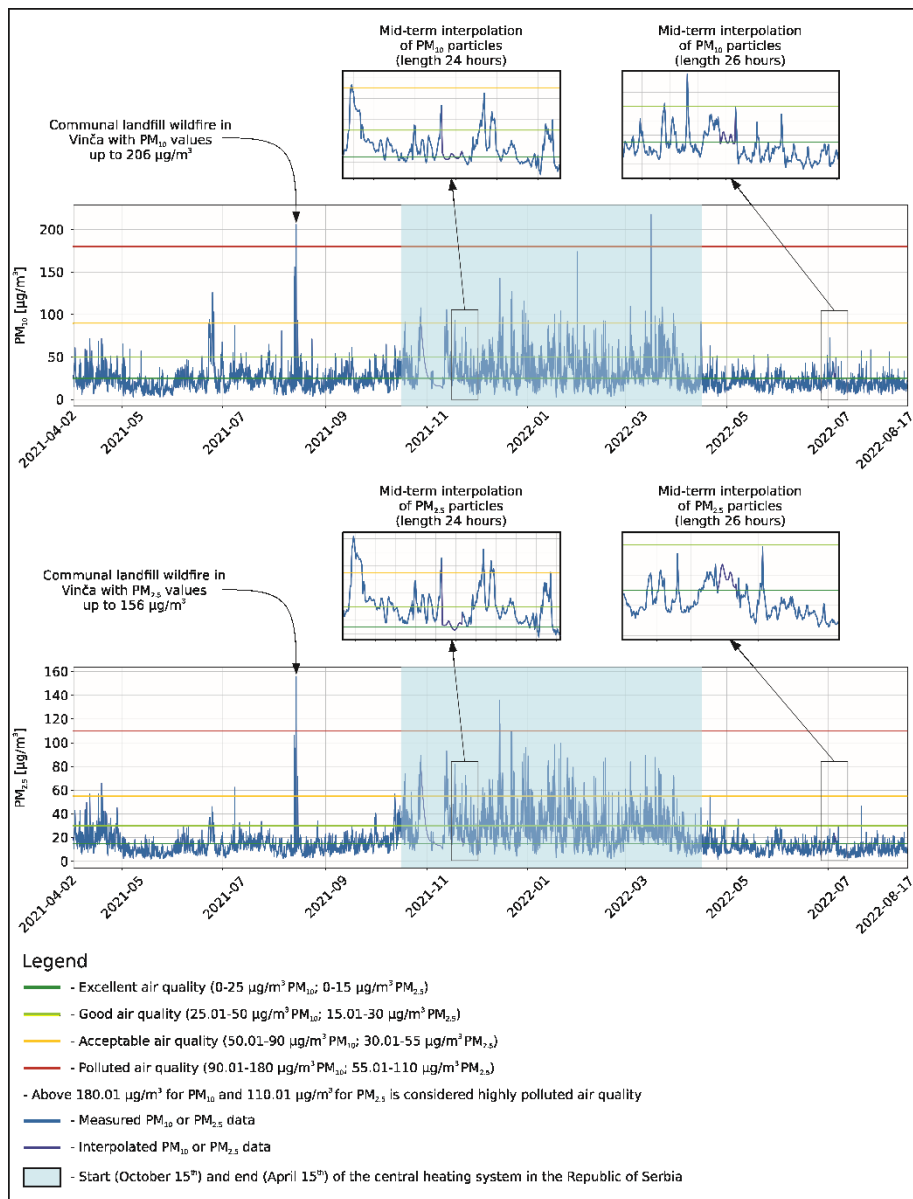
**Figure 3.** Processed PM₁₀ (*top*) and PM₂.₅ (*bottom*) data.

With the separation of data and the enabling of the central heating system, it was possible to express the same idea in a different way. In the RS, the central heating system is activated on October 15th and remains in

*Table 2. The air quality index and its duration at the monitoring station in Belgrade-Zeleno brdo during heating and non-heating season.*

| Air quality index | Non heating season PM$_{10}$ [h] | Heating season PM$_{10}$ [h] | Both heating and non-heating season PM$_{10}$ [h] |
|---|---|---|---|
| Excellent | 5456 | 1677 | 7133 |
| Good | 2050 | 1908 | 3958 |
| Acceptable | 176 | 714 | 890 |
| Polluted | 21 | 67 | 88 |
| Very polluted | 1 | 2 | 3 |
| Air quality index | Non heating season PM$_{2.5}$ [h] | Heating season PM$_{2.5}$ [h] | Both heating and non-heating season PM$_{2.5}$ [h] |
| Excellent | 5332 | 882 | 6214 |
| Good | 2167 | 1790 | 3957 |
| Acceptable | 188 | 1327 | 1515 |
| Polluted | 16 | 365 | 381 |
| Very polluted | 1 | 4 | 5 |

operation until April 15th. The data was separated into two categories, one for the period when the central heating was active and the other for the period when it was not active (Tab. 2). Even though the number of hours measured when the central heating system is active (4,386 hours or 36% of the data set) is significantly less than the number of hours measured when the central heating system is not active (7,704 hours or 64% of the data set), the majority of polluted, and very polluted air quality indexes for the PM$_{2.5}$ particles were accounted for by the data measured during active central heating. In contrast, the situation was less severe for PM$_{10}$ particles, where the ratio of heating season to non-heating season for the extremely polluted air quality index was 2:1. (for the PM$_{2.5}$ particles the ratio is 4:1). The ratio of polluted air quality indexes during the heating season to non-heating season was 23:1 (365:16) for PM$_{2.5}$ and 3:1 (67:21) for PM$_{10}$ particles.

In congruence with the correlation analysis displayed previously, when the annual temperature drops and households and the central heating system were active, a greater effect should be observed for PM$_{2.5}$ particles compared to PM$_{10}$ particles, and the material used for household heating has an undeniable impact on the air quality index at the Belgrade- Zeleno brdo measuring station.

### *3.2. Forecasting of PM$_{10}$ and PM$_{2.5}$ concentrations*

As both PM$_{10}$ and PM$_{2.5}$ values were provided as a single time series with a total length of 12,084 hours, forecasting was conducted using multiple shorter time series, each with a fixed 24-hour forecasting horizon (Fig. 4). This approach allowed for more forecasts with shorter time series, enabling a more comprehensive statistical validation of the selected model. Figure 4 depicts shorter time series, each with duration of 120 hours. The first step was the first 120 hours, or from April 2$^{nd}$ to April 6$^{th}$, 2021, with a forecast horizon of 24 hours, or the entire 7$^{th}$ of April. Five quantitative assessment parameters (*AE*, *MAE*, *APE*, *MAPE*, *RMSE*) and the forecasted value of PM$_{10}$ and PM$_{2.5}$ were the outputs of such a forecast. The next step was the next 120 hours, or from the 8$^{th}$ to the 12$^{th}$ of April, with the 13$^{th}$ of April being the forecasted and validation date. Such iterations are performed for the entire data set, with the length of n (in this case 120 hours). There were a total of 83 distinct time series and forecasts made for a 120 hour period. The length of the introductory time series was then extended from 120 hours to 240 hours and further until it covered the entire dataset of 12,048 hours.
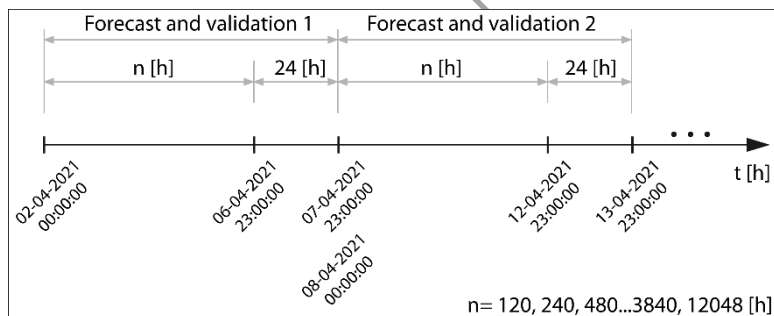


**Figure 4.** The principle of separating a time series into multiple shorter time series.

A parameter can be introduced that represents the ration of the introductory time series (number of historical data) relative to the length of the forecasting horizon. This ratio increases as the number of historical data ncreases while the forecasting horizon remains the same. For the introductory time series with a length of 120 hours and a forecasting horizon of 24 hours, the ratio was defined as 5:1, meaning that five historical data points were utilized to generate one future data point. The maximum value of such a ratio, however, was 501:1 when the introductory time series has a length of 12,048 hours, and the forecasting horizon was not altered. Table 3 presents such a ratio, the number of predictions made for the given ratio, and the minimum, mean, median, and maximum values of the *RMSE* calculated based on all

predictions made for the ratio. The ratio 12048:24 was excludes from Tab. 3 as it was described in greater detail individually.

*Table 3. Root mean square error for shorter time series.*

| Parameter | Ratio | Number of forecasts | $RMSE_{min}$ [µg/m$^3$] | $RMSE_{mean}$ [µg/m$^3$] | $RMSE_{median}$ [µg/m$^3$] | $RMSE_{max}$ [µg/m$^3$] |
|---|---|---|---|---|---|---|
| PM$_{2.5}$ | 120:24 (5:1) | 83 | 1.04 | 9.20 | 6.35 | 33.81 |
| | 240:24 (10:1) | 45 | 1.41 | 8.45 | 5.82 | 38.71 |
| | 480:24 (20:1) | 23 | 2.85 | 11.42 | 9.04 | 46.02 |
| | 960: 24 (40:1) | 12 | 1.96 | 10.49 | 8.29 | 31.03 |
| | 1920:24 (80:1) | 6 | 1.98 | 4.83 | 4.87 | 7.65 |
| | 3840:24 (160:1) | 3 | 2.00 | 6.24 | 3.78 | 12.93 |
| PM$_{10}$ | 120:24 (5:1) | 83 | 1.64 | 12.85 | 10.79 | 41.21 |
| | 240:24 (10:1) | 45 | 2.30 | 11.01 | 8.21 | 46.11 |
| | 480:24 (20:1) | 23 | 3.77 | 16.19 | 15.26 | 50.78 |
| | 960: 24 (40:1) | 12 | 3.77 | 15.23 | 11.52 | 49.25 |
| | 1920:24 (80:1) | 6 | 3.12 | 6.47 | 6.17 | 9.39 |
| | 3840:24 (160:1) | 3 | 4.49 | 8.97 | 7.04 | 15.39 |

The *RMSE* values obtained from Tab. 3 for PM$_{10}$ and PM$_{2.5}$ suspended particles suggest that the Prophet model may, in some cases, result in significant deviations between predicted and true values. In the case of a ratio of 480:24 for PM$_{10}$ concentration, the *RMSE* in one forecast was 50.78 µg/m$^3$. In that situation, the *MAE* was 49.54 µg/m$^3$ and the *MAPE* was 57.34%. The validation window for this time series, otherwise, contained values that were unexpectedly high. The mean PM$_{10}$ value for the validation window was about 85 µg/m$^3$, whereas the mean for the entire data set was 26.53 µg/m$^3$. In addition, for both the PM$_{10}$ and PM$_{2.5}$ parameters, an introductory time series of 1920 hours yielded the lowest calculated error parameters. Based on the number of predictions made for the given duration (6), it cannot be stated with a high degree of certainty that the event was not random. Additional modelling and forecasting should be done in the future to confirm the optimal length of the introductory time series for the Prophet model.

The mean *RMSE* values were lower for PM$_{2.5}$ particle concentrations across all ratios compared to PM$_{10}$, and the same holds true for the median *RMSE* value. The calculated *RMSE* values indicate that the model displayed more accurate PM$_{2.5}$ concentration values. Based on all 173 forecasts, 50% of forecasts will have a lower *RMSE* value than 6.26 µg/m$^3$ for PM$_{2.5}$ concentrations and 9.99 µg/m$^3$ for PM$_{10}$ concentrations.

Figure 5 depicts the forecast for the entire data set, using 12048 hours of data were used as the introductory time series to obtain 24-hour future values. Figure 5a depicts the PM$_{10}$ particle forecast, the *AE* and *APE* parameters. The *AE* fluctuates between 2 µg/m$^3$ and 10 µg/m$^3$, with a mean value of 6.5 µg/m$^3$. The *APE* ranges from 10.5% to 93.0%, with an average of 46.45%. Otherwise, as expected, the *AE* values for PM$_{2.5}$ particles were lower, ranging from 0.73 µg/m$^3$ to 5 µg/m$^3$ with a mean *MAE* of 2.7 µg/m$^3$. Similarly, the *MAPE* was less than the *MAPE* for PM$_{10}$ particles. High *APE* and *MAPE* values for PM$_{10}$ and PM$_{2.5}$ particles were not alarming. Even though the *AE* was small, the *APE* can be relatively large when predicting low values, demonstrating the inadequacy of using the two aforementioned errors. Figure 5b's 15$^{th}$ hour PM$_{2.5}$ particle forecast can be used as an example. The true value was 7.04 µg/m$^3$, while the predicted value was 8.84 µg/m$^3$. In this instance, the *AE* was relatively small at 1.8 µg/m$^3$, but the *APE* was high at 25%. The contrast also applies to the prediction of high values. As a result, we advise to calculate and display additional quantitative assessment parameters, which in this case was the *RMSE*. When interpreting *AE* and *APE* values, it is crucial to consider the predicted order of magnitude.

The quality of the Prophet model was also evident when displaying daily variations in PM$_{10}$ and PM$_{2.5}$ concentrations, an essential forecasting parameter. In both cases illustrated in Fig. 5, the model displayed daily PM$_{10}$ and PM$_{2.5}$ variations. While the predicted values may differ from the actual measurements, they adequately represent the general trend of daily concentration increases and decreases. The conformity of the true and forecasted curves from Fig. 5 can be adequately seen in the trend component, even though the values are not absolutely accurate. This research can be compared to the work of Shen et al. (2020); both studies agree that the Prophet model provides more accurate forecasts for PM$_{2.5}$ particles compared to PM$_{10}$ particles.

Future research in the field of PM$_{2.5}$ air quality forecasting could incorporate various novel forecasting techniques, including Uber's EN-RNN (Smyl, 2020), FFORMA (Manso et al., 2020), forecasHybrid (Shaub, 2020), and ShoTS (Thomakos et al., 2022), tailored for shorter time series and other time
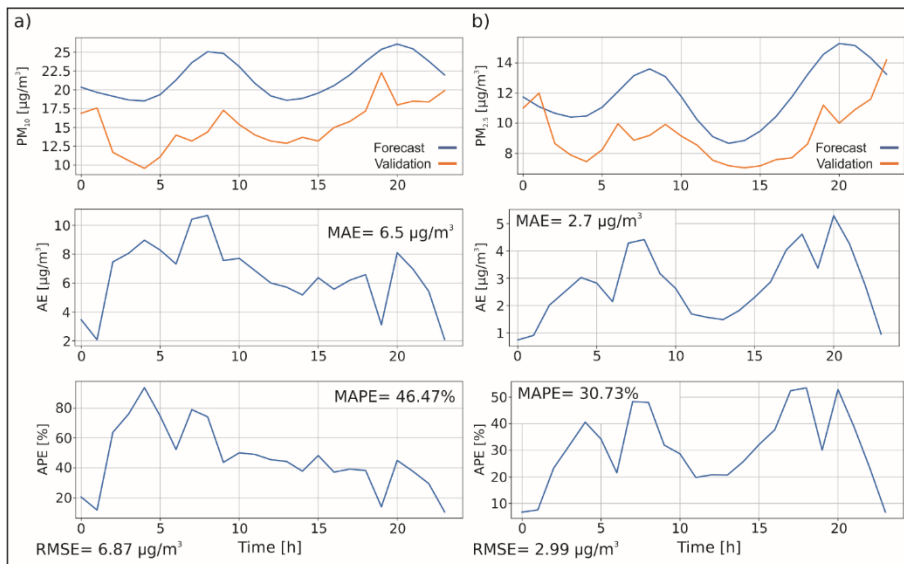
**Figure 5.** (*a*) Forecast of the $PM_{10}$ concentration, absolute and absolute percentage error; (*b*) Forecast of the $PM_{2.5}$ concentration, absolute and absolute percentage error.

series forecasting methods. Aside from conventional time series forecasting methods and machine learning techniques.

## 4. Conclusion

Accurately predicting future concentrations of suspended particles and other air quality parameters is crucial information that authorities can utilize to mitigate the risks of cardiovascular and respiratory diseases. In this research, the Prophet model was utilized for short-term (24- hour in advance) $PM_{10}$ and $PM_{2.5}$ particle forecasting. Based on 173 forecasts with varying lengths of the introductory time series, it is expected that Prophet model will produce *RMSE* values that are less than 6.26 μg/m$^3$ and 9.9 μg/m$^3$ for $PM_{2.5}$ and $PM_{10}$ particles, respectively.

The calculated error parameters for the longest introductory time series (12048 hours) confirmed that the *RMSE* is smaller for the $PM_{2.5}$ parameter (2.99 μg/m$^3$) than for the $PM_{10}$ parameter. (6.87 μg/m$^3$). Additionally, the Prophet model adequately reflected daily variations in $PM_{10}$ and $PM_{2.5}$ parameters, even though the values were not forecasted with absolute precision.

This research should not be interpreted as a stand-alone study, but rather as an introduction to a larger study that will include additional monitoring stations in Belgrade and other air quality parameters as well as hourly traffic conditions and other meteorological data. Furthermore, various models should be evaluated using various data transformation techniques (such as normalization and stationarity). Developing a method for accurate forecasts would unquestionably increase the likelihood of successfully mitigating air pollution, which could lead to a reduction in cardiovascular and respiratory diseases. Future research should also examine whether the Prophet model is suitable for longer-term forecasts.

# References

Agrawal, R. K. and Adhikari, R. (2013): *An introductory study on time series modeling and forecasting*. New York, CoRR, pp. 67, https://doi.org/10.48550/arXiv.1302.6613.

Araujo, J. A. (2011): Particulate air pollution, systemic oxidative stress, inflammation, and atherosclerosis, *Air Qual. Atmos. Health.*, **4**, 79–93, https://doi.org/10.1007%2Fs11869-010-0101-8.

Bernstein, J. A., Alexis, N., Barnes, C., Bernstein, I. L., Nel, A., Peden, D., Diaz-Sanchez, D., Tarlo, M. T. and Williams, P. B. (2004): Health effects of air polluion, *J. Allergy Clin. Immunol.*, **114**, 1116–1123, https://doi.org/10.1016/j.jaci.2004.08.030.

Bisgaard, S. and Kulahci, M. (2011): *Time series analysis and forecasting by example*. John Wiley & Sons, pp 400.

Dockery, D. W., Schwartz, J. and Spengler, J. D. (1992): Air pollution and daily mortality: associations with particulates and acid aerosols, *Environ. Res.*, **59**, 362–373, https://doi.org/10.1016/s0013-9351(05)80042-8.

Ejohwomu, O. A., Shamsideen Oshodi, O., Oladokun, M., Bukoye, O. T., Emekwuru, N., Sotunbo, A. and Adenuga, O. (2022): Modelling and forecasting temporal PM$_{2.5}$ concentration using ensemble machine learning methods, *Buildings*, **12**, 46, https://doi.org/10.3390/buildings12010046.

Energy Agency of the Republic of Serbia (2020): Report on the work of the Energy Agency for the year 2020. *Energy Agency of the Republic of Serbia* (In Serbian).

Environmental Protection Agency of th Republic of Serbia (2022): Air pollution index. *Environmental Protection Agency of the Republic of Serbia* (last accessed on 15 September 2022, available at: http://www.amskv.sepa.gov.rs/kriterijumi.php) (Online, in Serbian).

Hartigan, J. A. and Hartigan, P. M. (1985): The dip test of unimodality, *Ann. Stat.,* **13**, 70–84, https://doi.org/10.1214/aos/1176346577.

Hyndman, R. J. and Koehler, A. B. (2006): Another look at measures of forecast accuracy, *Int. J. Forecast.*, **22**, 679–688, https://doi.org/10.1016/j.ijforecast.2006.03.001.

Iowa Environmental Mesonet (2022): *Iowa Environmental Mesonet ASOS Network*. Iowa State University (last accessed on 15 September 2022, available at: https://mesonet.agron.iastate.edu/request/download.phtml.

Jovanović, M. V. (2020): *Chemical content and oxidative potential of respirable particulate matter in urban and in industrial environments*. PhD dissertation, Faculty of Chemsitry, University of Belgrade, pp 106.

Kang, H. (2013): The prevention and handling of the missing data, *Korean. J. Anesthiol.*, **64**, 402–406, https://doi.org/10.4097%2Fkjae.2013.64.5.402.

Kovačić, J. Z. (1995): *Time series analysis*. Faculty of Economics, University of Belgrade, pp 2 (In Serbian).

L. Zhoul, M. Chenl and Q. Ni. (2020): A hybrid Prophet-LSTM model for prediction of air quality index, *2020 IEEE Symposium Series on Computational Intelligence*. 595–601, https://doi.org/10.1109/SSCI47803.2020.9308543.

Lütkepohl, H. and Krätzig, M. (2004): *Applied time series econometrics*. Cambridge University Press, pp 323.

Montero-Manso, P., Athanasopoulos, G., Hyndman, R.J. and Talagala, T.S. (2020): FFORMA: Feature-based forecast model averaging, *Int. J. Forecast.*, **36**, 86–92, https://doi.org/10.1016/j.ijforecast.2019.02.011.

Official Gazette of the Republic of Serbia (156/2020): Decision on determining the energy balance of the Republic of Serbia for 2021 (156/2020).

Papastefanopoulos, V., Linardatos, P. and Kotsiantis, S. (2020): COVID-19: A comparison of time series methods to forecast percentage of active cases per population, *Appl, Sci.*, **10**(11), 3880, https://doi.org/10.3390/app10113880.

Puljić, V. M., Jones, D., Moore, C., Myllyvirta, L., Gierens, R., Kalaba, I., Ciuta, I., Gallop, P. and Risteska, S. (2019): *Chronic coal pollution – EU action in the Western Balkans will improve health and economies across Europe*. HEAL, CAN Europe, Sandbag, CEE Bankwatch Network i Europe Beyond Coal (In Serbian).

Samal, K. K. R., Babu, K. S., Das, S. K. and Acharaya, A. (2019): Time series based air pollution forecasting using SARIMA and prophet model, in: *Proceedings of the 2019 International Conference on Information Technology and Computer Communications,* 80–85, https://doi.org/10.1145/3355402.3355417.

Schober, P., Boer, C. and Schwarte, L. A. (2018): Correlation coefficients: appropriate use and interpretation, *Anesth. Analg.,* **126**, 1763–1768, 10.1213/ANE.0000000000002864.

Shakeel, A., Chong, D. and Wang, J. (2023a): Load forecasting of district heating system based on improved FB-Prophet model, *Energy*, **278**, 127637, https://doi.org/10.1016/j.energy.2023.127637.

Shakeel, A., Chong, D. and Wang, J. (2023b): District heating load forecasting with a hybrid model based on LightGBM and FB-prophet, *J. Clean. Prod.*, **409**, p. 137130, https://doi.org/10.1016/j.energy.2023.137130.

Shaub, D. (2020): Fast and accurate yearly time series forecasting with forecast combinations, *Int. J. Forecast.*, **36**, 116–120, https://doi.org/10.1016/j.ijforecast.2019.03.032.

Shen, J., Valagolam, D. and McCalla, S. (2020): Prophet forecasting model: a machine learning approach to predict the concentration of air pollutants (PM$_{2.5}$, PM$_{10}$, O$_3$, NO$_2$, SO$_2$, CO) in Seoul, South Korea. *Peer J.*, **8**, https://doi.org/10.7717%2Fpeerj.9961.

Smith, Taylor G., et al. (2017): pmdarima: ARIMA estimators for Python, http://www.alkaline-ml.com/pmdarima (Online; last accessed on 18 October 2023).

Smyl, S. (2020): A hybrid method of exponential smoothing and recurrent neural networks for time series forecasting, *Int. J. Forecast.*, **36**, 75–85, https://doi.org/10.1016/j.ijforecast.2019.03.017.

Taylor, S. J. and Letham, B. (2018): Forecasting at scale, *Am. Stat.*, **72**, 37–45, https://doi.org/10.1080/00031305.2017.1380080.

Tejasvini, K. N., Amith, G. R. and Shilpa, H. (2020): Air pollution forecasting using multiple time series approach, in: *Proceedings of the Global AI Congress 2019*, 91–100, https://doi.org/10.1007/978-981-15-2188-1_8.

Thomakos, D., Wood, G., Ioakimidis, M. and Papagiannakis, G. (2023): ShoTS forecasting: Short time series forecasting for management research, *Brit. J. Manage.*, https://doi.org/10.1111/1467-8551.12624

World Health Organization (2019): *Health impact of ambient air pollution in Serbia: A call to action.* World Health Organization.

Ye, Z. (2019): Air pollutants prediction in Shenzhen based on ARIMA and Prophet method, *E3S Web Conf.*, **136**, 1–5, https://doi.org/10.1051/e3sconf/201913605001.

Zhao, N., Liu, Y., Vanos, J. K. and Cao, G. (2018): Day-of-week and seasonal patterns of PM$_{2.5}$ concentrations over the United States: Time-series analyses using the Prophet procedure, *Atmos. Environ.*, **192**, 116–127, https://doi.org/10.1016/j.atmosenv.2018.08.050.

## SAŽETAK

# Kratkoročno predviđanje koncentracija PM$_{10}$ i PM$_{2.5}$ pomoću Facebookovog Prophet modela na Beograd-Zeleno brdo

*Filip Arnaut, Vesna Cvetkov, Dragana Đurić i Mileva Samardžić-Petrović*

Demonstriramo korištenje Facebookovog Prophet (obično samo Prophet) modela za kratkoročnu prognozu kvalitete zraka na mjernoj stanici Beograd-Zeleno brdo. Kako bismo riješili podatke koji nedostaju, primijenili smo tehnike imputacije podataka koje minimalno mijenjaju distribuciju. Linearna interpolacija pokazala se učinkovitom za kratkoročne praznine (1–3 sata), metoda satnih srednjaka za srednjoročne praznine (24–26 sati), a Hermite interpolacijski polinom za dugoročne praznine (132–148 sati). Najznačajnija promjena podataka bio je pomak od 3,4% u asimetričnosti. Podjelom vremenskog niza omogućena je detaljna procjena kvalitete modela Prophet, pri čemu su predviđanja PM$_{2.5}$ bila preciznija od PM$_{10}$. Korištenje najdužeg vremenskog niza za prognoziranje dalo je apsolutne pogreške od 6,5 μg/m$^3$ za PM$_{10}$ i 2,7 μg/m$^3$ za PM$_{2.5}$. Na temelju 173 predviđanja, predviđamo srednje kvadratne vrijednosti Prophetovog modela ispod 6,26 μg/m$^3$ i 9,99 μg/m$^3$ za PM$_{2.5}$ i PM$_{10}$ u 50% slučajeva. Model Prophet pokazuje nekoliko prednosti i daje zadovoljavajuće rezultate. U budućim istraživanjima, rezultati dobiveni iz Prophet modela poslužit će kao referentne vrijednosti za druge modele. Osim toga, model Prophet može pružiti zadovoljavajuće rezultate predviđanja kvalitete zraka i koristit će se u budućim istraživanjima.

*Ključne riječi:* analiza vremenskih nizova, predviđanje vremenskih nizova, kvaliteta zraka, lebdeće čestice.

*Corresponding author's address*: Filip Arnaut, Department of Geophysics, Faculty of Mining and Geology, University of Belgrade, Đušina 7, 11120 Belgrade, Serbia; tel: +381 63 83 89 237; e-mail: filip.arnaut@rgf.rs